EDGE ARTICLE

Phenylene segments of zigzag carbon nanotubes synthesized by metal-mediated dimerization†

Xuan-Wen Chen, Ke-Shan Chu, Rong-Jing Wei, Zhen-Lin Qiu, Chun Tang and Yuan-Zhi Tan [ID] *

Well-studied cycloparaphenylenes (CPPs) correspond to the simplest segments of armchair CNTs, whereas the corresponding macrocyclic oligophenylene strip of zigzag CNTs is still missing. Herein, we present two series of conjugated macrocycles (CM2PP and CN2PP) containing two *meta*-phenylene or 2,7-naphthylene units facing each other in the strip. CM2PP and CN2PP can be regarded as the shortest cyclic primitive segments of zigzag CNTs. They were synthesized by gold-mediated dimerization and unambiguously characterized. They adopted the tubular structures and can further pack into one-dimensional supramolecular nanotubes. In particular, the supramolecular nanotube of CM2P4P mimics the CNT(9, 0) structure. Structural analysis and theoretical calculation accounted for the reduced ring strain in CM2PPs and CN2PPs. CM2PPs and CN2PPs exhibited a large optical extinction coefficient and high photoluminescence quantum yield. CN2P8P can accommodate fullerene C_{60}, forming a Saturn-like C_{60}@CN2P8P complex, a mimic structure of zigzag CNT peapods.

Introduction

Carbon nanotubes (CNTs) are viewed as a layer of a rolled graphene sheet.[1] The vector along which the graphene sheet is rolled determines the chiral index (*n*, *m*) of CNTs. Accordingly, the CNTs are classified into three distinct types, armchair (*n* = *m*), chiral (*n* > *m* > 0), and zigzag (*n*, *m* = 0). Different types of CNTs exhibit dramatically different electronic and optical properties. Synthesis of CNTs with identical chiral indices is still an enduring challenge, although great attention has been paid and advances have been made in the last few decades.[2–5] Bottom-up rational synthesis starting from specific organic templates is one of the promising strategies to realize atomic precision.[6–10] Structurally, CNTs can be sliced into macrocycles composed of phenylene units, still maintaining the tubular and benzenoid characteristics.[11] For armchair (*n*, *n*)CNTs, cyclo-paraphenylenes (CPP[*n*]), formed by *para*-linked phenylenes, are the corresponding shortest macrocyclic segments[12] (Fig. 1). Axial π-extension of CPPs by organic synthesis can produce fully fused and elongated fragments of armchair CNTs.[13] Further, the armchair CNTs with a controllable diameter can be obtained by chemical vapor deposition (CVD) using CPPs as seeds.[14,15]

State Key Laboratory for Physical Chemistry of Solid Surfaces, Department of Chemistry, College of Chemistry and Chemical Engineering, Xiamen University, Xiamen 361005, China. E-mail: yuanzhi_tan@xmu.edu.cn

Although some fascinating and remarkable fully-fused macrocyclic segments of zigzag CNTs have been synthesized and reported very recently;[16–18] the macrocyclic oligophenylene strip of zigzag CNTs is still missing. Considering the *para* and *meta* connections between phenylene units, the macrocyclic cutouts of zigzag CNTs require at least two *meta*-linked aromatic units. Two embedded meta-linked aromatic units need to be located at opposite positions (Fig. 1). Different from the armchair CNTs, only zigzag CNTs with index (3*y*, 0) (*y* is an integer) can be sliced into fully phenylene macrocycles; the rest require at least one fused aromatic unit, such as naphthylene
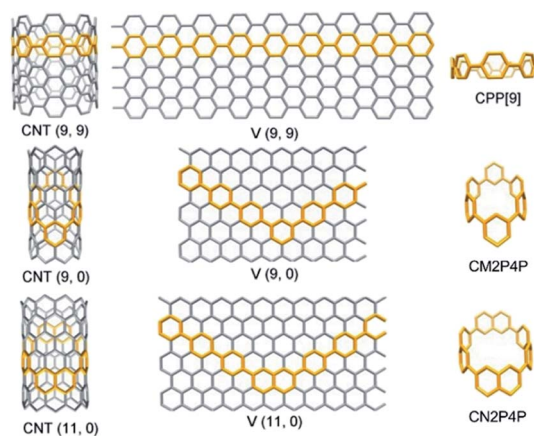

Fig. 1 The phenylene segments of CNTs, taking armchair CNT(9, 9), zigzag CNT(9, 0), and CNT(11, 0) as examples. CNT(*n*, *m*) can be unzipped into a graphene sheet defined by a vector [V(*n*, *m*)].

(Fig. 1 and S1†). Then the phenylene macrocycles of zigzag CNT(n, 0) are summarized as a molecular rosary with a general nomenclature, cyclo-naphthyl-2,7-ene(h)-meta(k)-para($2x$)-phenylene (CM[h]N[k]P[$2x$]P), with $x = [[n/3]] - 1$, $h = 2 - k$, and $k = n - 3[[n/3]]$. $[[n/3]]$ denotes the integer part of $n/3$ and x denotes the number of *para*-phenylene beads "P" that are separated and connected by h ($= 0$, 1 or 2) m-phenylene beads "M" and k ($=2$, 1 or 0) naphthyl-2,7-ene beads "N" (Fig. 1, S1† and Scheme 1).

The macrocycles bearing multiple *para*-phenylene units have strong ring strain, leading to difficulty in their synthesis. For example, the cyclic-*meta*-phenylenes were synthesized in the 1960s,[19] while CPPs were synthesized in the last decade.[20–22] To overcome the unfavorable strong ring strain, L-shaped synthons were used to construct the cyclic structures before the final aromatization.[20,21] This strategy produced a series of *para*-phenylene-containing macrocycles with different ring sizes and arene units,[23–25] but it requires a long synthetic route staring from commercial chemicals. Alternatively, a convenient platinum-mediated cyclotetramerization of CPPs was developed[26] and later improved[27] by replacing the toxic trimethyl tin with boronate esters. Platinum-mediated cyclotetramerization facilitated the synthesis of aromatic macrocycles with C_4 symmetry,[28] owing to the square-shaped coordination of the platinum complex. Using the angular arene units, platinum-mediated cyclization was changed from tetramerization to trimerization,[29,30] resulting in aromatic macrocycles with C_3 symmetry. Recently, gold-mediated cyclotrimerization was reported using the triangular coordination of the dinuclear gold complex,[31] providing a new strategy for aromatic macrocycles with C_3 symmetry.[32] Phenylene macrocyclic segments of zigzag CNTs, as shown in Scheme 1, have a C_2 symmetry when Ar1 = Ar2 (Scheme 1) and thus demand intermolecular cyclodimerization of repeating aromatic units. The intramolecular cyclodimerization of arene units could be achieved by Ni-catalyzed Yamamoto coupling.[33] However, the metal-mediated intermolecular assembly and cyclodimerization of phenylene macrocycles have not been reported before.

Results and discussion

Here, we show four phenylene macrocycles, CM2P4P, CM2P8P, CN2P4P, and CN2P8P, synthesized by gold-mediated intermolecular assembly and cyclodimerization. CM2P4P, CM2P8P, CN2P4P, and CN2P8P contain two *meta*-phenylene or 2,7-naphthylene units at opposite positions, linked by *para*-phenylene chains, representing the phenylene segments of CNTs with chiral indices (9, 0), (15, 0), (11, 0), and (17, 0), respectively.
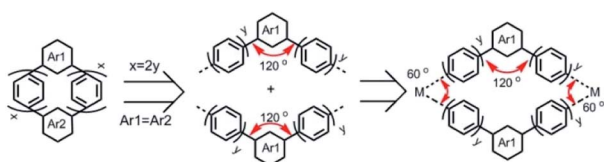
Scheme 1 Synthetic design of phenylene macrocyclic segments of zigzag CNTs.

The molecular structures of CM2P4P, CM2P8P, CN2P4P, and CN2P8P, studied by single-crystal X-ray diffraction (SCXRD), reveal an elliptical tubular shape, which further elongates with increasing ring size. They are packed into one-dimensional (1D) supramolecular nanotubes in the crystalline state, where the 1D supramolecular nanotube of CMP2P4P mimics the zigzag CNT (9, 0). They show an intense optical absorption and high photoluminescence quantum yield (PLQY). Furthermore, CN2P8P can host a fullerene C_{60}, forming a Saturn-like C_{60}@CN2P8P complex, structurally analogous to the zigzag CNT peapods.

As shown in Scheme 1, the phenylene cyclic segments of zigzag CNTs contain two *meta*-arene units at opposite positions. When Ar1 = Ar2 and $x = 2y$, this macrocycle can be divided into two symmetrical angular chains with an angle of 120°. Direct cycling of these two angular chains by Suzuki–Miyaura cross-coupling would produce the polymeric chains instead. Geometrically combining these two angular chains forms a rhombic cycle with an inter-chain angle of 60° (Scheme 1). This inter-chain angle fits the coordination geometry of dinuclear gold complexes, previously used for metal-mediated cyclotrimerization of linear arene units.[31,32] We propose that gold-mediated cyclotrimerization of linear arene units can be used to the cyclodimerization of angular arene building blocks.

Then, 1,3-di(4-diboronic acid dipinacol ester phenyl) benzene (compound **3**) is synthesized (ESI†) and reacted with [Au_2Cl_2(dcpm)] in degassed toluene/H_2O/EtOH at 50 °C to form a coordination macrocyclic intermediate (Fig. 2). The single crystals of this dinuclear gold complex were grown from the mixture by slow vapor diffusion of acetonitrile into 1,1,2,2-tetrachloroethane solution and then measured by SCXRD (Table S1†). The crystal structure of the gold-complex (Fig. 2) clearly showed a dimerized structure with an angle between two phenylene building units of 59.4°, which is consistent with our assumption. Sequentially, oxidative chlorination of the macrocyclic coordination intermediate is carried out by adding PhICl$_2$, leading to the formation of phenylene macrocycles (Fig. 2). After extracting with dichloromethane, the crude products were analyzed by high-resolution MALDI-TOF mass spectrometry. In the absence of other macrocycles with more repeating units, only the signals of dimerized macrocycle CM2P4P are observed (Fig. S2†). After purification, pure CM2P4P is obtained with a 31% yield over two steps.

Following a similar cyclodimerization strategy, CM2P8P with a larger ring size is synthesized with a yield of 16%. Considering the same substitution angle of 120° between *meta*-phenylene and 2,7-naphthylene substituents, the diboronic acid dipinacol ester of 2,7-naphthylene derivatives was also subjected to gold-mediated cyclodimerization, producing CN2P4P and CN2P8P with a yield of 19% and 12%, respectively. The mass spectra of CM2PPs and CN2PPs show dominant peaks that match the calculated isotopic pattern of their molecular formulae (Fig. S3–S6†). Their NMR spectra were recorded and found to be in agreement with their C_{2v} molecular symmetry (Fig. S7–S18†).

CM2PPs' and CN2PPs' single crystals were grown by slow vapor diffusion of hexane into carbon disulfide solution and then measured (Tables S2–S5†). As shown in Fig. 3, CM2P4P, CM2P8P, CN2P4P, and CN2P8P exhibit tubular structures,
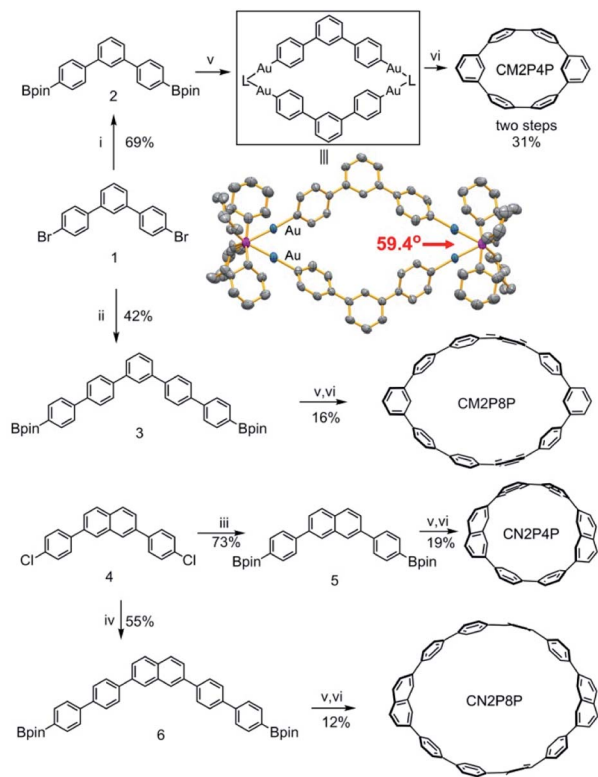
Fig. 2 Synthetic procedure for CM2P4P, CM2P8P, CN2P4P, and CN2P8P (L = bis(dicyclohexylphosphino)methane, dcpm). The crystal structure of the Au complex is in the inset and hydrogen atoms are omitted for clarity. Conditions and reagents: (i) bis(pinacolate)diboron (3 equiv.), KOAc (5 equiv.), Pd(dppf)Cl$_2$ (5 mol%), 1,4-dioxane, 80 °C, 12 h, 69%; (ii) 1,4-benzenediboronic acid bis(pinacol) ester (10 equiv.), Na$_2$CO$_3$ (15 equiv.), Pd(PPh$_3$)$_4$ (10 mol%), 1,4-dioxane/EtOH/H$_2$O (10 : 7 : 7), 80 °C, 12 h, 42%; (iii) bis(pinacolate)diboron (4 equiv.), KOAc (5 equiv), Pd$_2$dba$_3$ (5 mol%), Sphos (10 mol%), 1,4-dioxane, 80 °C, 12 h, 73%; (iv) 1,4-benzenediboronic acid bis(pinacol) ester (10 equiv.), Cs$_2$CO$_3$ (12 equiv.), Pd$_2$dba$_3$ (10 mol%), Sphos (20 mol%), DMF, 110 °C, 12 h, 55%; (v) [Au$_2$Cl$_2$(dcpm)] (1 equiv.), Cs$_2$CO$_3$ (6 equiv.), toluene/ EtOH/H$_2$O (4 : 1 : 1), 50 °C, 24 h; (vi) PhICl$_2$ (2 equiv.), DMF, 50 °C, 24 h.
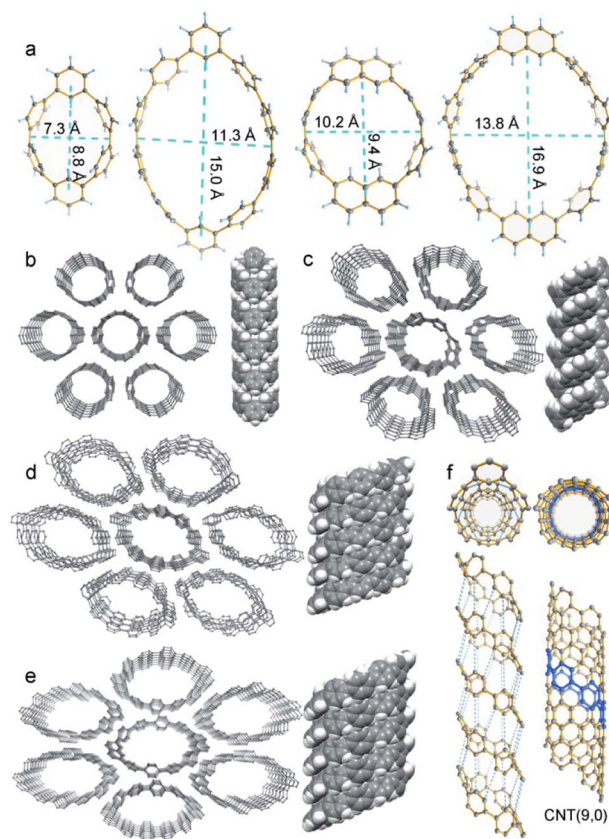

Fig. 3 Crystal structures of CM2P4P, CM2P8P, CN2P4P, and CN2P8P. (a) Top view of CM2P4P, CM2P8P, CN2P4P, and CN2P8P. The thermal ellipsoids are set at a probability level of 50%. (b) Packing structure of CM2P4P. (c) Packing structure of CN2P4P. (d) Packing structure of CM2P8P. (e) Packing structure of CN2P8P. (f) Comparison between the CM2P4P supramolecular tube and CNT (9, 0). The blue dashed lines represent the connection between the carbon atoms from the neighboring rings. Hydrogen atoms are omitted for clarity.

analogous to those of CNTs. The *para*-phenylene units adopt a conformation nearly perpendicular to the plane of the macrocycle. Structural extension of CM2PPs and CN2PPs along their π-plane will form infinite zigzag CNTs, and thus CM2P4P, CM2P8P, CN2P4P, and CN2P8P can be regarded as the primitive segments of zigzag CNTs with chiral indices (9, 0), (15, 0), (11, 0), and (17, 0), respectively. CM2P4P exhibits an elliptical conformation with a long and short axis of 8.8 and 7.3 Å. The conformation of CM2P8P becomes more elliptical with a long and short axis of 15.0 and 11.3 Å (Fig. 3a). In comparison, the size of CN2PPs is slightly larger and their structure is less elliptical, attributed to the incorporation of larger and rigid naphthylene units (Fig. 3a). The *para*-phenylene rings in CM2P4P and CN2P4P are bent away from the planar structure with an average angle of 10.3° and 9.6°, smaller than that of CPP [6] (12.7°),[34] indicating their reduced ring strain. In larger rings CM2P8P and CN2P8P, the bent angle dramatically decreases to 6.2° and 6.0°, indicating a sharp strain release. The ring strain,

calculated at the B3LYP/6-31G(d,p) level, is 52.3 and 52.5 kcal mol^{-1} for CM2P4P and CN2P4P (Fig. S35 and Table S7†), which are smaller than that of CPP[6] owing to the introduction of two less strained *meta*-linked arene units.[34] The ring strain of CM2P8P and CN2P8P decreases sharply to 29.4 and 29.6 kcal mol^{-1}, consistent with the geometrical analysis.

SCXRD data also reveal the supramolecular assembly of CM2P4P, CM2P8P, CN2P4P, and CN2P8P. All of them are packed into 1D supramolecular tubes (Fig. 3b–e). These 1D supramolecular tubes are arranged into a quasi-hexagonal columnar packing, forming continuous 1-D channels (Fig. 3b–e), which could be used for gas absorption and separation.[35] In particular, the 1D supramolecular tubes of CM2P4P have an identical connection of carbon atoms to that of zigzag CNT(9, 0), when connecting the carbon atoms from the neighboring CM2P4P (Fig. 3f). This supramolecular structure of CM2P4P hints the possibility of forming well-defined CNT(9, 0) by coupling these molecular cutouts together when CM2P4P was functionalized with reactive groups such as halogen atoms.[36]

Tubular structures of CM2P4P, CM2P8P, CN2P4P, and CN2P8P make them soluble in organic solvents. In chloroform,

CM2P4P shows an absorption peak at 304 nm with a maximum extinction coefficient (ε_{max}) of 2.8×10^4 M^{-1} cm^{-1} (Fig. 4), blue-shifted by 34 nm compared with CPP[6]. Increasing the ring size to CM2P8P, the optical absorption peak shifts to 320 nm with a ε_{max} of 5.9×10^4 M^{-1} cm^{-1}. The maximum absorption of CN2P4P and CN2P8P occurs at 282 and 303 nm with a ε_{max} of 2.7×10^4 and 5.2×10^4 M^{-1} cm^{-1}, respectively. The absorption ability is enhanced with increasing ring size (Fig. 4), consistent with the cases of CPPs. However the optical emission of CM2P4P, CM2P8P, CN2P4P, and CN2P8P is found at 374, 405, 410, and 412 nm, respectively, in proportion with the ring size (Fig. 4), which is different from the cases of CPPs.[23] The PLQYs of CM2P4P, CM2P8P, CN2P4P, and CN2P8P are 0.47, 0.91, 0.54, and 0.93, measured by the absolute method using an integrating sphere, which are higher than those of the corresponding CPPs and mCPPs.[23,24] High PLQY and large extinction coefficient indicate their potential in bioimaging and photoelectronics.

On the other hand, the tubular structures of CM2P4P, CM2P8P, CN2P4P, and CN2P8P can host the guest molecules by supramolecular interactions. As revealed by SCXRD, CM2P4P and CN2P4P accommodate one carbon disulfide molecule inside, while the enlarged ring sizes of CM2P8P and CN2P8P enable the capsulation of more complex guests, such as fullerenes. By adding equimolar C_{60} in CM2P8P or CN2P8P solution, obvious shifts in the proton signals are observed in the mixture of CN2P8P and C_{60}, indicating the formation of a supramolecular complex of CN2P8P and C_{60} (Fig. 5 and S31†). The UV-Vis spectrum of the mixture of CN2P8P and C_{60} did not show changes corresponding to the formation of the complex (Fig. S33†), owing to the weak charge-transfer between CN2P8P and C_{60}. Job plot analysis based on NMR titration revealed the formation of 1:1 complexes in solution (Fig. S32†). The detailed structure of the CN2P8P and C_{60} complex is obtained by SCXRD (Table S7†). As shown in Fig. 5, C_{60} is located at the center of CN2P8P, forming a Saturn-like supramolecular complex C_{60}@CN2P8P and mimicking the zigzag CNT peapods.[37] The short axis of the ring in the complex increases slightly to 14.3 Å
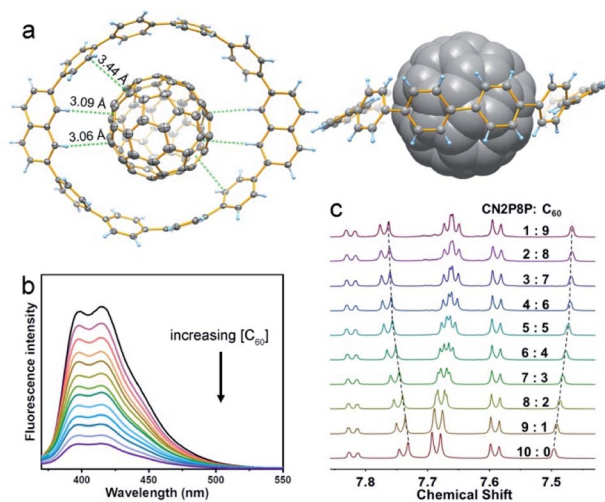
Fig. 5 Supramolecular assembly between CN2P8P and C_{60}. (a) Structure of C_{60}@CN2P8P. The top view is plotted in an ellipsoid model at the probability level of 50%. The intermolecular short distances are represented by green dashed lines. The side view is represented in space-filling and ball-and-stick models; (b) fluorescence spectra of CN2P8P (λ_{exc} = 305 nm) in the presence of C_{60} in toluene. (c) ^{1}H NMR spectra (600 MHz, 298 K) during titration of CN2P8P with C_{60} in 1,1,2,2-tetrachloroethane-d2.

from 13.8 Å in free CN2P8P, revealing a structural match between C_{60} and CN2P8P. The shortest distance from the π-sphere of C_{60} to CN2P8P in C_{60}@CN2P8P is 3.43 Å (Fig. 5a), comparable with C_{60}@CPP[10] (3.37 Å).[37] In addition to π–π interactions, hydrogen atoms of the naphthylene units are pointed to the phenyl ring of C_{60} with a distance of 3.06 Å (Fig. 5a), indicating C–H⋯π interactions, which assist the formation of the C_{60}@CN2P8P complex. NMR and fluorescence titration reveal that the binding constant of C_{60}@CPP[10] is $(1.6 \pm 0.3) \times 10^3$ M^{-1} and $(1.8 \pm 0.4) \times 10^3$ M^{-1}, respectively, obtained by non-linear least-squares analysis (Fig. 5b, c, S32 and S34†), which is smaller than that of C_{60}@CPP[10] $[(6.0 \pm 0.2) \times 10^3$ M$^{-1}]$.[37]

Conclusions

In summary, four phenylene macrocycles CM2P4P, CM2P8P, CN2P4P, and CN2P8P were synthesized by gold-mediated dimerization. Structurally, CM[h]N[k]P[2x]P represented the phenylene segments of zigzag CNTs. In the solid-state, 1D supramolecular tubes of CM2P4P, CM2P8P, CN2P4P, and CN2P8P were formed. Among them, 1D supramolecular assembly of CM2P4P mimicked the tubular structure of CNT(9, 0). Bright deep-blue emission of these macrocycles renders them intriguing fluorophores. Their hosting ability was demonstrated by the formation of C_{60}@CN2P8P, which can be regarded as the shortest zigzag CNT peapods. Facile synthesis of CM2P4P, CM2P8P, CN2P4P, and CN2P8P could help their further applications, for example, a template to synthesize fully-fused fragments of zigzag CNTs, seeds for CVD growth of zigzag CNTs, hosts for supramolecular assembly, and absorbents for
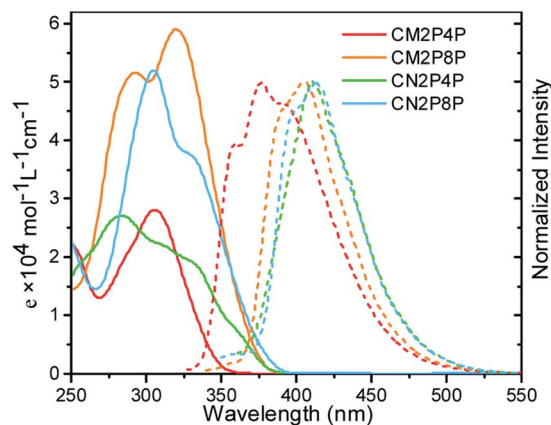

Fig. 4 Optical properties of CM2P4P, CM2P8P, CN2P4P, and CN2P8P in CHCl$_3$. The absorption and emission spectra are represented by solid and dashed lines, respectively.

gas absorption and separation. Gold-mediated dimerization of angular-shaped arene units could be further used to synthesize other interesting conjugated macrocycles.

Data availability

All supporting data are provided in the ESI.†

Author contributions

X.-W. C., K.-S. C. and R.-J. W. performed the experiments and measurements; X.-W. C. and C. T. did the DFT calculations; Z.-L. Q. and Y.-Z. T. carried out the X-ray crystallographic studies; Y.-Z. T. conceived the research hypothesis; all authors were involved in the preparation of the manuscript.

Conflicts of interest

The authors declare no conflict of interest.

Acknowledgements

Notes and references

1 M. S. Dresselhaus, G. Dresselhaus and R. Saito, *Carbon*, 1995, **33**, 883–891.
2 F. Yang, X. Wang, M. Li, X. Liu, X. Zhao, D. Zhang, Y. Zhang, J. Yang and Y. Li, *Acc. Chem. Res.*, 2016, **49**, 606–615.
3 F. Yang, M. Wang, D. Zhang, J. Yang, M. Zheng and Y. Li, *Chem. Rev.*, 2020, **120**, 2693–2758.
4 S. Zhang, X. Wang, F. Yao, M. He, D. Lin, H. Ma, Y. Sun, Q. Zhao, K. Liu, F. Ding and J. Zhang, *Chem*, 2019, **5**, 1182–1193.
5 K. Kogashi, T. Matsuno, S. Sato and H. Isobe, *Angew. Chem., Int. Ed.*, 2019, **58**, 7385–7389.
6 X. Yu, J. Zhang, W. Choi, J.-Y. Choi, J. M. Kim, L. Gan and Z. Liu, *Nano Lett.*, 2010, **10**, 3343–3349.
7 J. R. Sanchez-Valencia, T. Dienel, O. Groening, I. Shorubalko, A. Mueller, M. Jansen, K. Amsharov, P. Ruffieux and R. Fasel, *Nature*, 2014, **512**, 61–64.
8 B. Liu, J. Liu, H.-B. Li, R. Bhola, E. A. Jackson, L. T. Scott, A. Page, S. Irle, K. Morokuma and C. Zhou, *Nano Lett.*, 2015, **15**, 586–595.
9 L. T. Scott, E. A. Jackson, Q. Zhang, B. D. Steinberg, M. Bancu and B. Li, *J. Am. Chem. Soc.*, 2012, **134**, 107–110.
10 Q.-H. Guo, Y. Qiu, M.-X. Wang and J. Fraser Stoddart, *Nat. Chem.*, 2021, **13**, 402–419.
11 S. E. Lewis, *Chem. Soc. Rev.*, 2015, **44**, 2221–2304.
12 Y. Segawa, A. Yagi, K. Matsui and K. Itami, *Angew. Chem., Int. Ed.*, 2016, **55**, 5136–5158.
13 K. Y. Cheung, S. Gui, C. Deng, H. Liang, Z. Xia, Z. Liu, L. Chi and Q. Miao, *Chem*, 2019, **5**, 838–847.
14 H. Omachi, T. Nakayama, E. Takahashi, Y. Segawa and K. Itami, *Nat. Chem.*, 2013, **5**, 572–576.
15 B. Liu, F. Wu, H. Gui, M. Zheng and C. Zhou, *ACS Nano*, 2017, **11**, 31–53.
16 K. Y. Cheung, K. Watanabe, Y. Segawa and K. Itami, *Nat. Chem.*, 2021, **13**, 255–259.
17 Y. Han, S. Dong, J. Shao, W. Fan and C. Chi, *Angew. Chem., Int. Ed.*, 2021, **60**, 2658–2662.
18 Z. Xia, S. H. Pun, H. Chen and Q. Miao, *Angew. Chem., Int. Ed.*, 2021, **60**, 10311–10318.
19 H. A. Staab and F. Binnig, *Tetrahedron Lett.*, 1964, **5**, 319–321.
20 R. Jasti, J. Bhattacharjee, J. B. Neaton and C. R. Bertozzi, *J. Am. Chem. Soc.*, 2008, **130**, 17646–17647.
21 H. Takaba, H. Omachi, Y. Yamamoto, J. Bouffard and K. Itami, *Angew. Chem., Int. Ed.*, 2009, **48**, 6112–6116.
22 M. Hermann, D. Wassy and B. Esser, *Angew. Chem., Int. Ed.*, 2021, **60**, 15743–15766.
23 E. R. Darzi and R. Jasti, *Chem. Soc. Rev.*, 2015, **44**, 6401–6410.
24 T. C. Lovell, C. E. Colwell, L. N. Zakharov and R. Jasti, *Chem. Sci.*, 2019, **10**, 3786–3790.
25 Z.-L. Qiu, D. Chen, Z. Deng, K.-S. Chu, Y.-Z. Tan and J. Zhu, *Sci. China: Chem.*, 2021, **64**, 1004–1008.
26 S. Yamago, Y. Watanabe and T. Iwamoto, *Angew. Chem., Int. Ed.*, 2010, **49**, 757–759.
27 S. Hitosugi, T. Yamasaki and H. Isobe, *J. Am. Chem. Soc.*, 2012, **134**, 12442–12445.
28 Z.-L. Qiu, C. Tang, X.-R. Wang, Y.-Y. Ju, K.-S. Chu, Z.-Y. Deng, H. Hou, Y.-M. Liu and Y.-Z. Tan, *Angew. Chem., Int. Ed.*, 2020, **59**, 20868–20872.
29 H. Zhao, L. Cao, S. Huang, C. Ma, Y. Chang, K. Feng, L. L. Zhao, P. Zhao and X. Yan, *J. Org. Chem.*, 2020, **85**, 6951–6958.
30 K. Kogashi, T. Matsuno, S. Sato and H. Isobe, *Angew. Chem., Int. Ed.*, 2019, **58**, 7385–7389.
31 Y. Tsuchido, R. Abe, T. Ide and K. Osakada, *Angew. Chem., Int. Ed.*, 2020, **59**, 22928–22932.
32 Z.-L. Qiu, M.-b. He, K.-S. Chu, C. Tang, X.-W. Chen, L. Zhu, L.-P. Zhang, D. Sun, J. Qian and Y.-Z. Tan, *Adv. Opt. Mater.*, 2021, **9**, 2100482.
33 G. Ohlendorf, C. W. Mahler, S. S. Jester, G. Schnakenburg, S. Grimme and S. Hoger, *Angew. Chem., Int. Ed.*, 2013, **52**, 12086–12090.
34 J. Xia and R. Jasti, *Angew. Chem., Int. Ed.*, 2012, **51**, 2474–2476.
35 E. J. Leonhardt, J. M. Van Raden, D. Miller, L. N. Zakharov, B. Aleman and R. Jasti, *Nano Lett.*, 2018, **18**, 7991–7997.
36 W. Liu, X. Luo, Y. Bao, Y. P. Liu, G.-H. Ning, I. Abdelwahab, L. Li, C. T. Nai, Z. G. Hu, D. Zhao, B. Liu, S. Y. Quek and K. P. Loh, *Nat. Chem.*, 2017, **9**, 563–570.
37 T. Iwamoto, Y. Watanabe, T. Sadahiro, T. Haino and S. Yamago, *Angew. Chem., Int. Ed.*, 2011, **50**, 8342–8344.